Stoch Environ Res Risk Assess
DOI 10.1007/s00477-015-1065-x

ORIGINAL PAPER

Long-term periodic drought modeling

Jaber Almedeij[1]

Abstract Drought modeling is essential to water resources management and planning. In this study, Fourier spectral analysis is used to examine the cyclic structure for drought patterns and develop a long-term periodic model. A case study for historical precipitation data, obtained from the arid region of Kuwait for the period spanning from January 1967 to December 2009, are converted to drought measurements following the Standardized Precipitation Index (SPI) criterion. The SPI calculations are performed for two time scales of 12 and 24 months. The periodogram technique used for both time scales reveals periodicities of 12, 14, 19, 26, 31, 43, 64, 103 and 258 months. It is advocated here that the 26- and 258-month periods present in the data are attributed, respectively, to a Quasi-Biennial Oscillation pattern and a solar cycle over which the magnetic polarity of the sun first reverses then reverts to its former state. The detected periods are manipulated in the SPI model to produce drought forecasts, which suggest that until the end of year 2024 the climate is considered normal to very wet. This finding may be implemented to assess policy requirements related to water resources management.

Keywords SPI · Periodicity · Drought risk assessment · Arid region · Sunspots

✉ Jaber Almedeij
j.almedeij@ku.edu.kw

[1] Civil Engineering Department, Kuwait University, P.O. Box 5969, Safat, 13060 Kuwait, Kuwait

1 Introduction

Drought is a phenomenon, which may affect areas located in wet or dry environments, resulting in insufficient moisture due to a deficit in precipitation over a given time period (McKee et al. 1993). A thorough review of drought definitions was conducted by Wilhite and Glantz (1985), who classified drought into six categories based on meteorological, climatic, atmospheric, agricultural, hydrologic and water management features. The time scale over which precipitation deficits accumulate is important to elucidate these classifications. For example, agricultural droughts have typically a short-time scale of 1 month when soil moisture and rainfall cannot support crop growth and lead to yield losses (Lakshmi et al. 2004; Liu and Hwang 2015), whereas hydrologic droughts have intermediate- and long-time scales of 3, 6, 12 and 24 months with marked surface and subsurface water depletion from lakes, streams, reservoir or groundwater (Szalai et al. 2000; Van Loon et al. 2014). Reduced surface and subsurface water levels due to hydrologic drought increase water shortage risks, especially when water demand increases in all major use sectors due to population and economic growth (Bannayan and Hoogenboom 2014).

A widely acceptable index that has been used to assess and monitor drought characteristics quantitatively is the Standardized Precipitation Index (SPI) (McKee et al. 1993, 1995; Mishra and Singh 2010). The SPI criterion represents the difference of precipitation from the mean divided by the standard deviation, where these two statistical parameters are determined from past continuous records, ideally of at least 30 years (McKee et al. 1993). Owing to the reason that this index is standardized, it can be used to assess global drought impacts (e.g., Manatsa et al. 2010; Naresh Kumar et al. 2012). For a given location, the SPI

Published online: 01 April 2015

may also be computed for any time scale whether short, intermediate or long by simply estimating the probability distribution function for the time scale selected (Abarghouei et al. 2011). This feature will be instrumental to address effects of the abovementioned drought categories.

Drought forecasting is a critical component of water resources risk management (Cebrián and Abaurrea 2012). For Kuwait, a long-term drought model is useful to evaluate groundwater recharge capacities and water shortage risks. This was justified by Almedeij (2014), who constructed bivariate probability distributions for drought severity and duration using Clayton copula and frequency analysis. Although a short-term drought assessment is vital in many locations, it is not considered here, as the country does not rely on rainfall to support agricultural surfaces, rather it depends on nonconventional water resources such as seawater desalination and wastewater treatment and reuse. Mishra and Singh (2011) reviewed the advantages and limitations of various drought modeling and forecasting methodologies, including regression, time series, probability, neural network and hybrid models. They suggested that a long-term drought forecasting is possible by using climate indices and a model relying on the periodic nature of the data.

The aim of this study is to use SPI criterion to model drought patterns determined from historical rainfall records for Kuwait and to provide possible forecasts. The computation of SPI values will consider long-term scales of 12 and 24 months, generating average characteristics that are more reliable than short-term scales. The cyclical structure for SPI values will be examined in the frequency domain using the periodogram technique. A sinusoidal model that employs the results from the periodogram technique will then be developed.

1.1 Case study

The climate of Kuwait is arid, where rainstorms are infrequent with short duration but torrential. The average depth of annual evaporation is high, approaching a value of 4000 mm, while the annual depth of rainfall is low, varying from 35 to 242 mm. Summer (winter) temperatures reach an average daily high of 43 °C (15 °C) and an average daily low of 23 °C (5 °C). Summer temperatures can even be higher when hot winds blow from the desert. Winter temperatures are classified as mild but occasionally become cold when northerly or north-westerly winds bring cold air from the north.

Kuwait's arid environment causes water shortage problems. Essentially, the only existing conventional water resource is fresh groundwater with relatively limited quantities. The limited groundwater quantities are due to the few areas of actual surface water runoff and accumulation, as evaporation always exceeds available precipitation. Fresh groundwater is found in depressions of Rawdatain and Umm Al-Aish located in the northern area of Kuwait (Kwarteng et al. 2000). Freshwater from Rawdatain is reserved, with a portion marketed as bottled mineral water, and water from Umm Al-Aish was contaminated following a massive crude oil spill by the retreating Iraqi army during the 1990 Gulf War (Mukhopadhyay et al. 2008). Nonconventional water resources have become essential to overcome existing water shortage problems in the country (Alhumoud et al. 2003). Two alternative approaches, seawater desalination and wastewater treatment and reuse, have been applied. However, these approaches come with relatively high water production costs, and seawater desalination, which relies on multi-stage flash, causes environmental issues (Darwish and Al Awadhi 2009).

Monthly total rainfall data for Kuwait are used in this study to perform a drought analysis that will facilitate fresh groundwater monitoring activities. Owing to the relatively small land area, the average data for monthly total rainfall collected over the urban catchments of Kuwait from the weather stations shown in Fig. 1 are nearly equivalent (Almedeij 2012). These rainfall data are presented graphically in Fig. 2 showing small differences of ± 3 mm. Accordingly, rainfall data collected for a point estimate can be considered spatially representative. The monthly total rainfall data from the weather station at Kuwait International Airport, which has the longest range of rainfall records among the other stations, can be employed here for the analysis. The data are plotted in Fig. 3 for the period January 1967 to December 2009, with 516 monthly observations. It should be noted that data measurements for August 1990 to June 1991 were not recorded at the weather station because of the Iraqi invasion of Kuwait. To maintain time period continuity, this lack of information has been handled here by considering the seasonal mean produced by adding the value for the same month of the years before and after and then dividing this value by two.

2 SPI calculation and results

The SPI index is equivalent to the Z-score often used in statistics. However, in many cases, the distribution of rainfall measurements is considered skewed. Thom (1958) found that the gamma distribution fits rainfall data more appropriately. The probability density function for the gamma distribution $g(x)$ is defined as

$$g(x) = \frac{1}{\beta\Gamma(\alpha)} x^{\alpha-1} e^{-x/\beta} \quad (1)$$

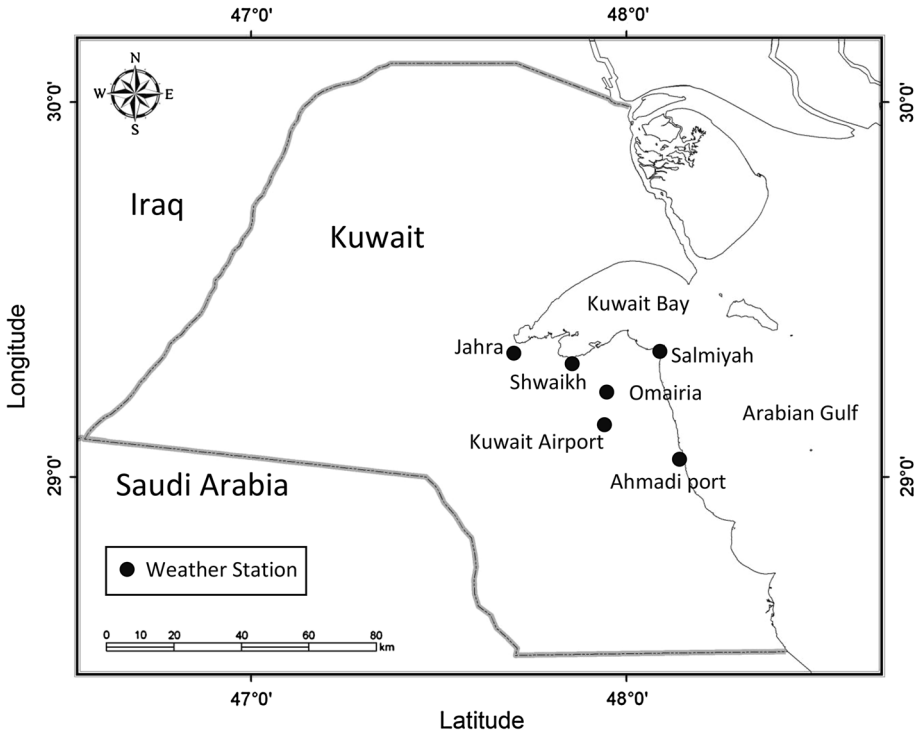

Fig. 1 Weather stations in urban areas of Kuwait

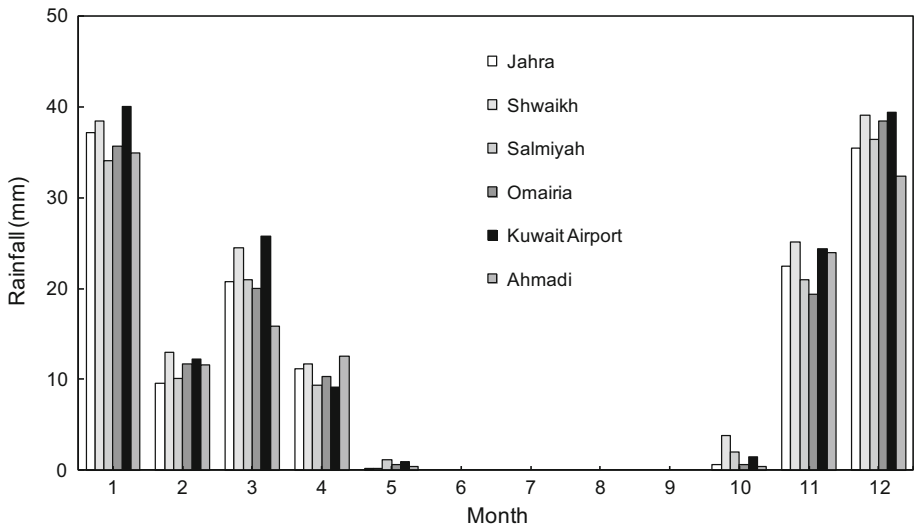

Fig. 2 Seasonal mean of monthly total rainfall collected from different weather stations over the urban catchments of Kuwait for the time duration from January 1994 to December 2005

where $\alpha > 0$ is the shape parameter, $\beta > 0$ is the scale parameter, and x is the rainfall measurement. The gamma function $\Gamma(\alpha)$ shown in the above equation is defined as

$$\Gamma(\alpha) = \int_0^\infty y^{\alpha-1} e^{-y} dy \tag{2}$$

Fitting the gamma distribution to rainfall data involves estimating α and β. Edwards and McKee (1997) recommended estimating these parameters using Thom's (1958) maximum likelihood approximation to obtain

$$\hat{\alpha} = \frac{1}{4A}\left(1 + \sqrt{1 + \frac{4A}{3}}\right) \tag{3}$$

$$\hat{\beta} = \frac{\bar{x}}{\hat{\alpha}} \tag{4}$$

where

$$A = \ln(\bar{x}) - \frac{\sum \ln(x)}{n} \tag{5}$$

n is the number of rainfall measurements, and $\bar{x}$ is the mean of x.

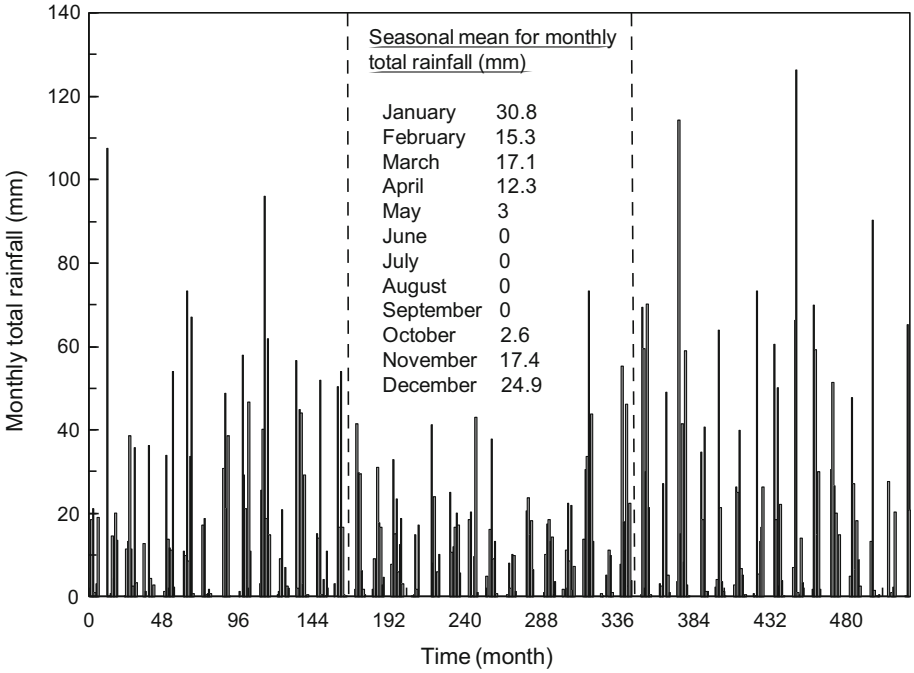

Fig. 3 Rainfall data obtained for January 1967 (month number 1) to December 2009 (month number 516). The two *dashed lines* divide the data into three equal time intervals at April 1981 (month number 172) and August 1995 (number 344)

Integrating $g(x)$ with respect to x and inserting estimates of α and β yields the cumulative distribution $G(x)$ expression for a given month and time scale

$$G(x) = \int_0^x g(x)dx = \frac{1}{\hat{\beta}^{\hat{\alpha}}\Gamma(\hat{\alpha})}\int_0^x x^{\hat{\alpha}-1}e^{-\frac{x}{\hat{\beta}}}dx \tag{6}$$

Assuming $t = x/\hat{\beta}$, this cumulative distribution becomes

$$G(x) = \frac{1}{\Gamma(\hat{\alpha})}\int_0^x t^{\hat{\alpha}-1}e^{-t}dt \tag{7}$$

As the gamma function is undefined for $x = 0$, and rainfall data may contain no measurements, the cumulative distribution may be conveniently expressed as

$$H(x) = q - (1-q)G(x) \tag{8}$$

where q represents the probability of a value of zero. That is, if m denotes the number of zero measurements recorded in a rainfall time series, Thom (1958) states that q can be estimated from m/n. The cumulative distribution $H(x)$ is then transformed into standard normal random variable Z employing the approximate conversion provided by Abramowitz and Stegun (2012) as

$$Z = SPI = -\left(t - \frac{c_0 + c_1 t + c_2 t^2}{1 + d_1 t + d_2 t^2 + d_3 t^3}\right) \quad \text{for} \quad 0 < H(x) \le 0.5 \tag{9}$$

$$Z = SPI = +\left(t - \frac{c_0 + c_1 t + c_2 t^2}{1 + d_1 t + d_2 t^2 + d_3 t^3}\right) \quad \text{for} \quad 0.5 < H(x) < 1.0 \tag{10}$$

where

$$t = \sqrt{\ln\left(\frac{1}{H(x)^2}\right)} \quad \text{for} \quad 0 < H(x) \le 0.5 \tag{11}$$

$$t = \sqrt{\ln\left(\frac{1}{1.0 - H(x)^2}\right)} \quad \text{for} \quad 0.5 < H(x) < 1.0 \tag{12}$$

The coefficients in Eqs. (9) and (10) are equal to $c_0 = 2.515517$, $c_1 = 0.802853$, $c_2 = 0.010328$, $d_1 = 1.432788$, $d_2 = 0.189269$ and $d_3 = 0.001308$.

The above criterion is used here to estimate SPI values for Kuwait rainfall data. Figure 4 shows the results presented as probability distribution functions for the time scales of 12 and 24 months. Here, the SPI values are referred to as SPI12 and SPI24. It is seen that the probability distributions are close to normal based on Anderson–Darling normality test, which produced minor statistics that do not reject the normality hypothesis for the p value at the 0.05 significance level. SPI classifications with regard to dry and wet events and the percentage available in each category in the time scales selected for Kuwait data are shown in Table 1. The SPI values are arbitrarily divided here into categories ranging from extremely wet (relative to the mean and standard deviation of the data) to extreme drought. The percentage available in the theoretical standard normal distribution is also presented for a comparison with the categories for Kuwait data.

The temporal behavior of SPI values is presented in Fig. 5. It is evident that drought intensities are highly variable and become less than −1.0 and greater than 1.0 on several occasions. These variations are attributable to the

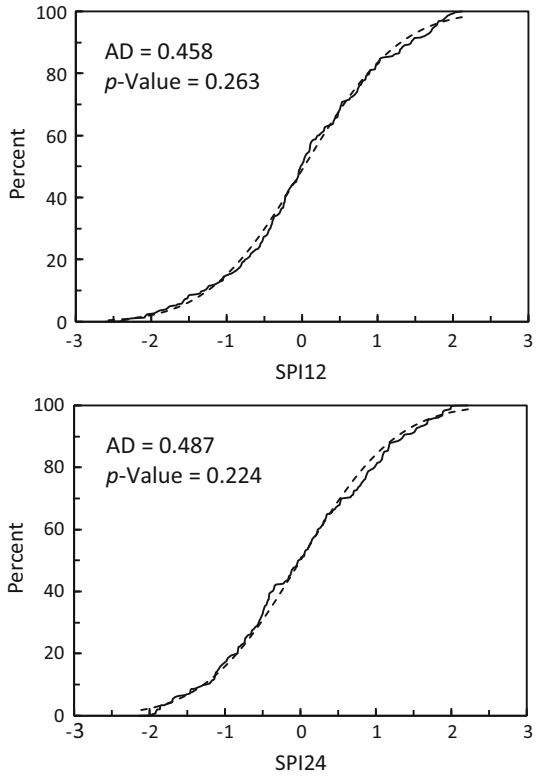

Fig. 4 SPI data plotted as probability distribution functions. The *dashed curve* represents the theoretical cumulative distribution, and the solid curve is the fitted empirical cumulative distribution. AD corresponds to the Anderson–Darling statistic

Table 1 SPI values and classifications

Class	SPI value[a]	Percentage in category (%)		
		SND[b]	SPI12	SPI24
Extremely wet	>2.0	2.28	0.78	0.39
Very wet	1.5 to 1.99	4.40	7.75	8.33
Moderately wet	1.0 to 1.49	9.19	8.72	10.27
Normal	0.99 to −0.99	68.26	67.64	63.57
Moderate drought	−1.0 to −1.49	9.19	6.40	10.27
Severe drought	−1.5 to −1.99	4.40	6.00	6.98
Extreme drought	<−2.0	2.28	2.71	0.19

[a] SPI categories adopted from Bordi et al. (2001)

[b] Standard normal distribution

seasonal nature of rainfall data. It is worth mentioning that the characteristics of the four seasons of Spring, Summer, Autumn and Winter are not distinct in the arid environment of Kuwait, which can rather be classified into rainy and dry months. Figure 3 shows that rainy months in Kuwait typically include November, December, January, February, March and April. Drought patterns appear largely after these months and grow worse during summer, *i.e.,* June, July and August. However, on a larger scale, dividing the rainfall data in Fig. 3 into three distinct equal time intervals of 172 months shows that the middle interval has lower rainfall levels than the others; total rainfall levels from the first to the third interval accumulate to 1870, 1420 and 2160 mm, respectively. One long-term drought clearly presented in the SPI24 series endures for approximately 10 years from December 1982 (month number 192) to January 1993 (month number 313). This drought event resulted from the low rainfall levels for the second time interval.

Figure 5 also shows no obvious long-term trend component. This can be tested by fitting a linear regression trend to the data, producing slope and intercept values nearly equal to zero. Validating this observation though requires the review of a sufficiently wider historical rainfall data series that is not available from this weather station. Such testing could determine whether a phenomenon such as climate change affects drought severity or frequency in the area.

2.1 Model development

The SPI data can be used to model drought variability. Generally, time series data are represented with a decomposition model of additive type composed of deterministic and stochastic components. The deterministic component accounts for trend and periodic features and can be formulated in a manner that supports exact predictions. The trend shows a long movement of the variable lasting over the entire time of observations, while the periodic part shows oscillating movement repetitive over a specific time interval. The stochastic component of time series data can never be estimated precisely, as it is formed by random effects. Although stochastic components are deemed sufficiently stationary in simple time series models, in most commonly considered situations, they present complex statistical correlations.

Although visual inspections for the given range of SPI12 and SPI24 data for Kuwait suggests an absence of trends with only periodic deterministic component, statistical inferences may be used to provide verification. This analysis can be accomplished using a single series of annual total rainfall from which both SPI datasets are directly derived. The claim to be tested is that a linear relation exists between the annual rainfall and time at a significance level of $\alpha = 0.05$ As shown in Fig. 6, the p-value for the slope of the fitted linear relation is 0.499. This means that there is a 0.499 probability of obtaining a slope estimate that is extreme or more extreme than that obtained if the null hypothesis of no linear relation was true. As the p-value is greater than the level of significance, the null hypothesis of no linear relation is accepted.

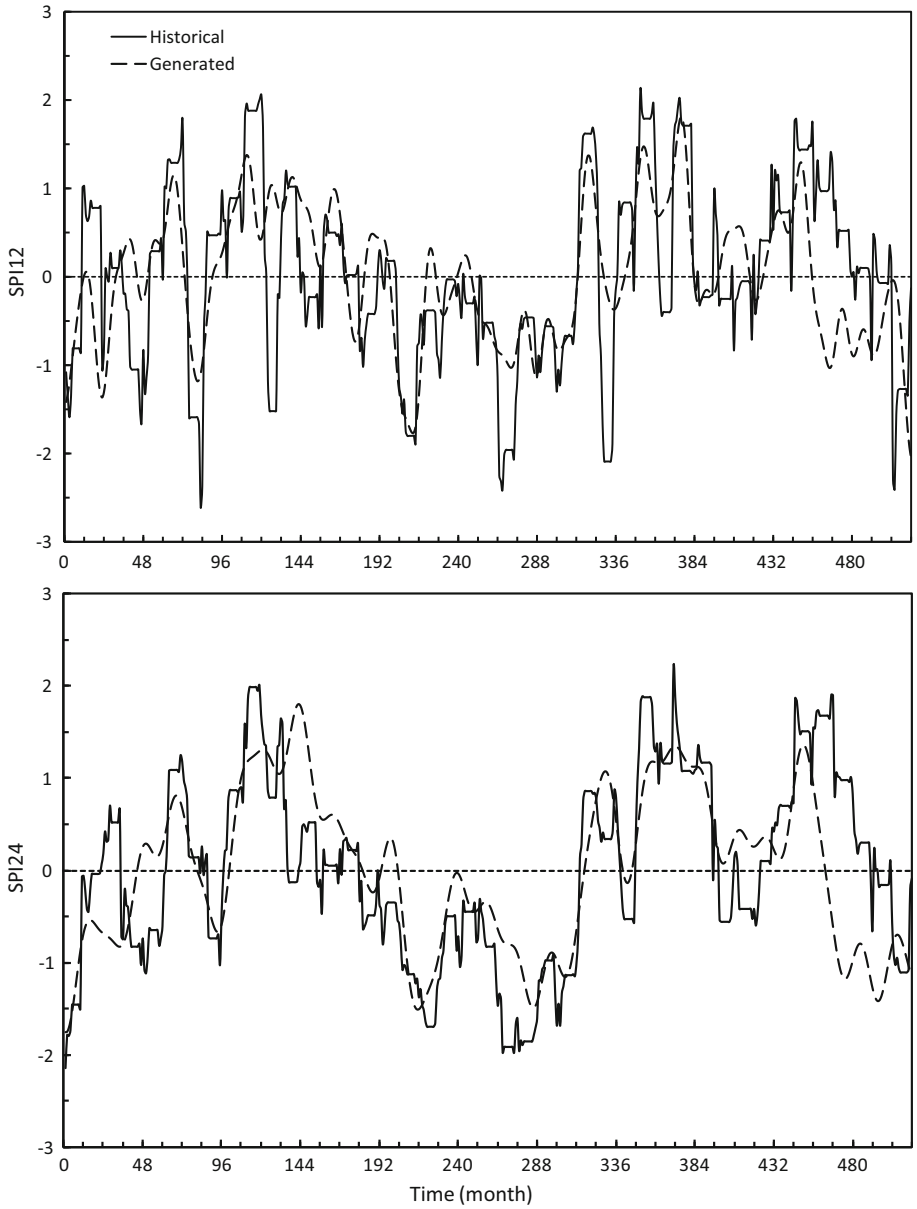

Fig. 5 SPI data versus time for January 1967 (month number 1) to December 2009 (number 516)

The patterns for SPI12 and SPI24 data can be examined by plotting a periodogram, which is a Fourier transform of the autocovariance function representing an unsmoothed spectral plot used to examine the cyclical structure of the frequency domain (Brockwell and Davis 2002). This technique is used to reduce measurement noise effects and thus to detect which frequencies for the range of time have the most influence on the data pattern. Typically, a large peak value in a periodogram corresponds with a period that is strongly represented in the time series. For example, a typical periodogram for monthly averaged temperature data can show a period of 12 months, implying that 6 months of the year exhibit considerably lower temperatures than the other 6 months.

Figure 7 presents periodograms for the two SPI datasets. Both periodograms show periods such as of 19, 26, 31, 43, 64, 103 and 258 months. However, the SPI12 periodogram also accounts for shorter periods of 12 and 14 months. It is worth obtaining the periodogram for the rainfall data as in Fig. 8. It is evident that the periods identified in the rainfall pattern are similar to those found in both SPI datasets, with magnitudes of 12, 18, 26, 30, 42, 64, 103 and 258 months. Overall, the existence of those periods suggests unclear climate variations. However, the 12-month period can certainly be related to a seasonal variation pattern typically observed in climatological data. It can also be noted that the 26-month period is attributed to well-known Quasi-Biennial Oscillation (QBO) patterns in zonal winds, a

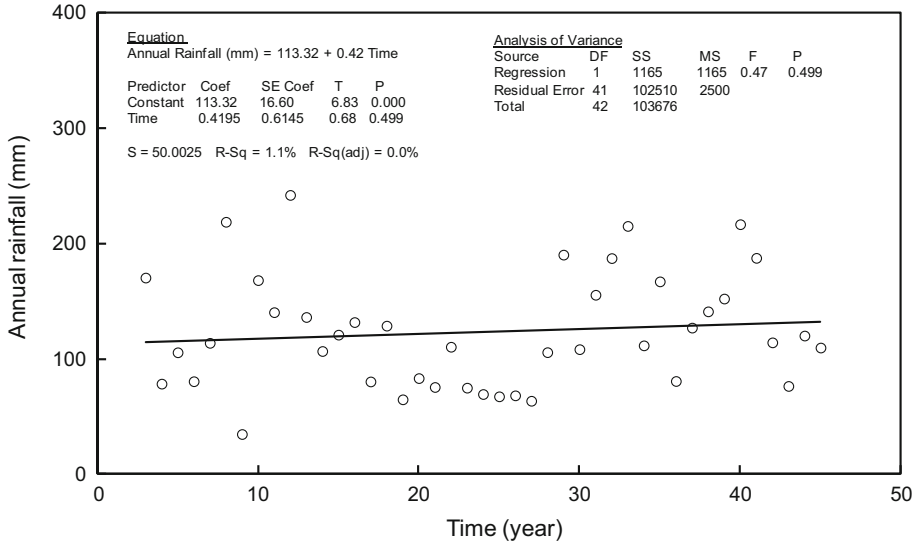

Fig. 6 Annual total rainfall versus time for year 1967 (year number 1) to 2009 (number 43). The *solid line* represents a trend fitted for the data via linear regression

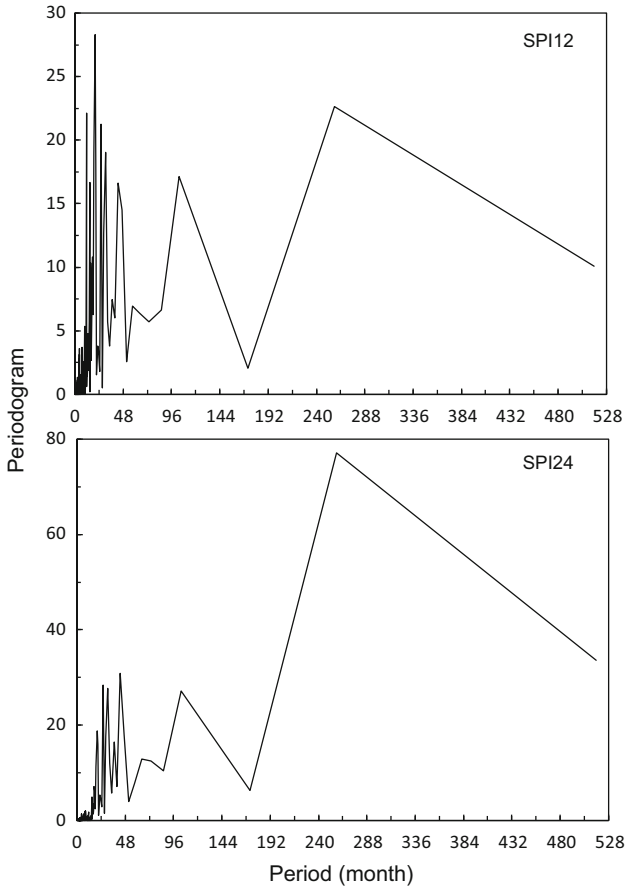

Fig. 7 Periodograms for SPI data obtained for January 1967 (month number 1) to December 2009 (number 516)

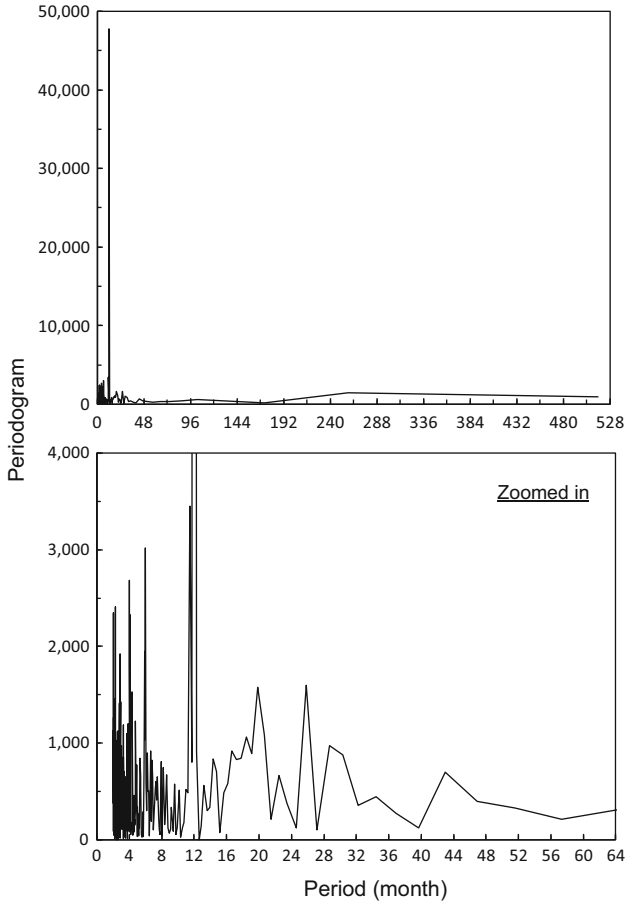

Fig. 8 Periodogram for monthly total rainfall data obtained for January 1967 (month number 1) to December 2009 (number 516)

dominant natural oscillation in the equatorial lower stratosphere (Almedeij and Al-Ruwaih 2006). The QBO involves a reversal of wind directions; that is, the prevailing wind direction is easterly for one year and then westerly for the following year (Angell and Korshover 1964).

The 258-month period is similar to a fundamental solar cycle with an average duration of 22 years, over which the magnetic polarity of the sun first reverses then reverts to its former state. When Newell et al. (1989) matched this solar cycle and temperature cycle, they found that the alternate peaks of the 11-year sunspot cycle correspond to alternate upward and downward swings of temperatures, suggesting that cooling takes place during one phase of solar magnetic polarity and warming during the other. Mitchell et al. (1979) reported that the 22-year solar periodicity modulates terrestrial drought-inducing mechanisms that encourage and discourage the development of major continental droughts.

The patterns for the SPI datasets can be estimated from the detected periods. In general, time-based data with a periodic sinusoidal component of known wavelength can be modeled using Fourier series, which can be expressed for multiple periods as

$$s(t) = \sum_{n=1}^{\infty} \sum_{i=1}^{k} R_{n,i} \cos\left(2n\pi f_i t + \theta_{n,i}\right) \tag{13}$$

where

$$R_{n,i} = \sqrt{a_{n,i}^2 + b_{n,i}^2}$$

$$\theta_{n,i} = \tan^{-1}\left(-\frac{b_{n,i}}{a_{n,i}}\right)$$

$$a_{n,i} = 2f_i \int_{L_i}^{L_i+\frac{1}{f_i}} f(x)\cos(2n\pi f_i t)dx$$

$$b_{n,i} = 2f_i \int_{L_i}^{L_i+\frac{1}{f_i}} f(x)\sin(2n\pi f_i t)dx$$

where s is the periodic sinusoidal component of SPI; R is the amplitude of variation; f is the frequency equal to the inverse of the period; θ is the phase angle; and k is the total number of periodicities. The term $(2n\pi ft + \theta)$ is measured in radians. As determined from the data, the k value is equal to seven and five for SPI12 and SPI24, respectively, and f values may be set by their periodic nature, *i.e.*, for SPI12, $f_1 = 1/12, f_2 = 1/14, f_3 = 1/19\ldots$ cycles per month. The phase angle, θ, is needed to adjust the model so that the cosine function crosses the mean, which is equal to zero for the data at the appropriate time t. The difficulty is to determine analytically the function $f(x)$ in Fourier coefficients. However, due to the presence of existing randomness, a more simple procedure may be followed by determining $\theta_{n,i}$ and $R_{n,i}$ by means of numerical optimization. As the above equation cannot be solved analytically, it is more convenient to reduce the number of fitting coefficients. This is achieved by testing a number of $s(t)$ models each obtained by assuming a different value of n. Following the Fourier procedure, larger n values produce higher degrees of model accuracy. In this case, however, greater accuracy would produce a more complex model form, as numerous periods are detected in the data. Thus, for simplicity, $n = 1$ is used. Following the above procedure, a model $s(t)$ for each SPI dataset can be developed in Fig. 5, with coefficients shown in Table 2. Here, in this figure, it is seen that the model fits the data with some variations that represent a remaining stochastic time series component.

The accuracy of the two models is evaluated in Fig. 9, which plots SPI12 and SPI24 datasets against corresponding generated values. Here, the solid line represents the condition of perfect agreement, and the dashed lines represent discrepancy values of $\Delta\text{SPI} = \mp 1$. The percentages of data for SPI12 and SPI24 falling within these discrepancy values are 82.36 and 84.50 %, respectively.

Given that conditions used to derive the model remain the same, drought forecasts can be performed. The span of a period can tell, to some extent, how far in time the model can provide forecasts. Because the longest period employed in the model is of 258 months (21.5 years), forecasts can possibly be provided from January 2010 until December 2030 as in Fig. 10. According to the classifications defined in Table 1, average SPI values for January 2014 (month number 565) to December 2024 (month number 696) are considered normal to very wet. The implication is that the model can be used to produce potential drought forecasts in order to assess critical policy requirements related to water resources management.

Table 2 Estimated coefficients for $s(t)$ models with n = 1

i	f_i	SPI12		SPI24	
	(1/month)	$R_{n,i}$	$\theta_{n,i}$	$R_{n,i}$	$\theta_{n,i}$
1	1/12	−0.11	0.31	0.00	0.00
2	1/14	−0.10	3.50	0.00	0.00
3	1/19	−0.23	−1.38	−0.14	−0.31
4	1/26	0.31	3.54	0.10	2.54
5	1/31	−0.37	1.63	0.28	2.92
6	1/43	0.36	3.47	0.29	2.70
7	1/64	−0.34	4.31	−0.38	3.29
8	1/103	0.35	3.96	0.44	3.71
9	1/258	0.70	3.31	0.98	3.17

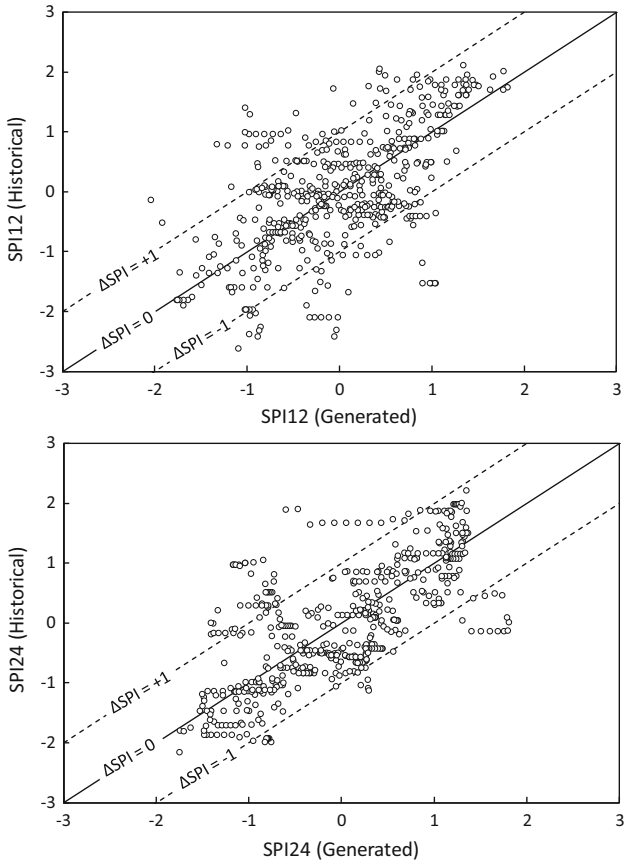

Fig. 9 Historical versus generated SPI data

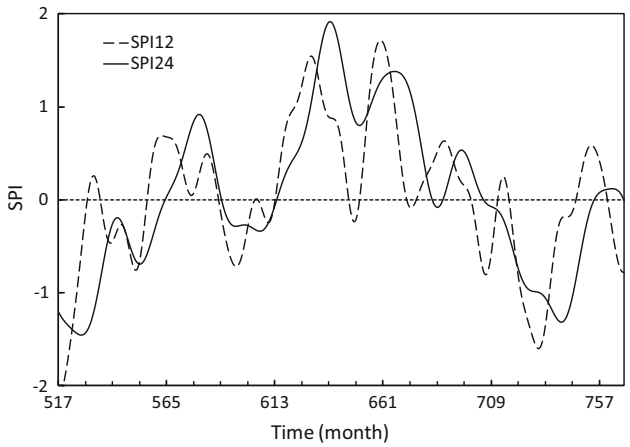

Fig. 10 SPI model forecasts obtained for January 2010 (month number 517) to December 2030 (number 768)

3 Conclusions

This study has found that the examined SPI datasets for Kuwait have no trend, but only obvious periodic patterns. Finding a trend would justify whether a phenomenon such as climate change affects drought severity or frequency in the area. The periodogram technique revealed distinct periods, some of which are similar to those found in QBO and solar activity patterns. This similarity indicates a possible connection of droughts with persistent phenomena that can be exploited to produce a long-term drought model. The developed sinusoidal models for SPI12 and SPI24 were able to describe the data patterns with some discrepancies representing a remaining stochastic time series component. A wider range of data would thus be necessary to verify the accuracy of the revealed periods, unhide any other ones, and detect a possible trend in order to enhance the performance of the developed models.

Acknowledgments The author is grateful to the Directorate General of Civil Aviation of Kuwait for providing rainfall data. This work was supported by Kuwait University, Research Grant No. (EV09/13).

References

Abarghouei HB, Zarch MAA, Dastorani MT, Kousari MR, Zarch MS (2011) The survey of climatic drought trend in Iran. Stoch Env Res Risk Assess 25(6):851–863

Abramowitz M, Stegun IA (2012) Handbook of mathematical functions with formulas, graphs, and mathematical tables. Courier Dover Publications, New York

Alhumoud JM, Behbehani HS, Abdullah TH (2003) Wastewater reuse practices in Kuwait. Environmentalist 23(2):117–126

Almedeij J (2012) Modeling rainfall variability over urban areas: a case study for Kuwait. Sci World J. doi:10.1100/2012/980738

Almedeij J (2014) Drought analysis for Kuwait using Standardized Precipitation Index. Sci World J. doi:10.1155/2014/451841

Almedeij J, Al-Ruwaih F (2006) Periodic behavior of groundwater level fluctuations in residential areas. J Hydrol 328:677–684

Angell JK, Korshover J (1964) Quasi-biennial variations in temperature, total ozone, and tropopause height. J Atmos Sci 21(5):479–492

Bannayan M, and Hoogenboom G (2014) Quantification of agricultural drought occurrence as an estimate for insurance programs. Theor Appl Climatol 1–10

Bordi I, Frigio S, Parenti P, Speranza A, Sutera A (2001) The analysis of the standardized precipitation index in the Mediterranean area: large-scale patterns. Ann Geophys 44(5/6):965–978

Brockwell PJ, Davis RA (2002) Introduction to time series and forecasting. Springer, New York

Cebrián AC, Abaurrea J (2012) Risk measures for events with a stochastic duration: an application to drought analysis. Stoch Env Res Risk Assess 26(7):971–981

Darwish MA, Al Awadhi FM (2009) The need for integrated water management in Kuwait. Desalin Water Treatment 11:204–214

Edwards DD, and McKee TB (1997) Characteristics of 20th Century drought in the United States at multiple time series. Master thesis, Colorado State University

Kwarteng AY, Viswanathan MN, Al-Senafy MN, Rashid T (2000) Formation of fresh ground-water lenses in northern Kuwait. J Arid Environ 46(2):137–155

Lakshmi V, Piechota T, Narayan U, Tang C (2004) Soil moisture as an indicator of weather extremes. Geophys Res Lett 31(11):1–4

Liu Y, Hwang Y (2015) Improving drought predictability in Arkansas using the ensemble PDSI forecast technique. Stoch Env Res Risk Assess 29(1):79–91

Manatsa D, Mukwada G, Siziba E, Chinyanganya T (2010) Analysis of multidimensional aspects of agricultural droughts in Zimbabwe using the Standardized Precipitation Index (SPI). Theoret Appl Climatol 102(3–4):287–305

McKee TB, Doesken NJ, and Kleist J (1993) The relationship of drought frequency and duration to time scales. Proceedings of the 8th conference on applied climatology, American Meteorological Society, Boston

McKee TB, Doesken NJ, and Kleist J (1995) Drought monitoring with multiple time scales. Proceedings of the 9th conference on applied climatology, American Meteorological Society, Boston

Mishra AK, Singh VP (2010) A review of drought concepts. J Hydrol 391(1):202–216

Mishra AK, Singh VP (2011) Drought modeling–a review. J Hydrol 403(1):157–175

Mitchell JM Jr, Stockton CW, Meko DM (1979) Evidence of a 22-year rhythm of drought in the western United States related to the Hale solar cycle since the 17th century. In: McCormac BM, Soliga TA (eds) Solar—terrestrial influences on weather and climate. Riedel Publications, Dordrecht

Mukhopadhyay A, Al-Awadi E, Quinn M, Akber A, Al-Senafy M, Rashid T (2008) Ground water contamination in Kuwait resulting from the 1991 gulf war: a preliminary assessment. Ground Water Monit Rem 28(2):81–93

Naresh Kumar M, Murthy CS, Sesha Sai MVR, Roy PS (2012) Spatiotemporal analysis of meteorological drought variability in the Indian region using standardized precipitation index. Meteorol Appl 19(2):256–264

Newell NE, Newell RE, Hsiung J, Zhongxiang W (1989) Global marine temperature variation and the solar magnetic cycle. Geophys Res Lett 16(4):311–314

Szalai S, Szinell C, Zoboki J (2000) Drought monitoring in Hungary. Early Warning Systems for Drought Preparedness and Drought Management, Geneva

Thom HCS (1958) A note on the gamma distribution. Mon Weather Rev 86(4):117–122

Van Loon AF, Tijdeman E, Wanders N, Van Lanen HA, Teuling AJ, Uijlenhoet R (2014) How climate seasonality modifies drought duration and deficit. J Geophys Res: Atmos 119(8):4640–4656

Wilhite DA, Glantz MH (1985) Understanding: the drought phenomenon: the role of definitions. Water Intern 10(3):111–120